



Role of a ribosomal RNA phosphate oxygen during the EF-G-triggered GTP hydrolysis

Miriam Koch^{a,1}, Sara Flür^{b,1}, Christoph Kreutz^b, Eric Ennifar^c, Ronald Micura^{b,2}, and Norbert Polacek^{a,2}

^aDepartment of Chemistry and Biochemistry, University of Bern, 3012 Bern, Switzerland; ^bInstitute of Organic Chemistry, Center for Molecular Biosciences Innsbruck, University of Innsbruck, 6020 Innsbruck, Austria; and ^cArchitecture et Réactivité des ARN, CNRS/Université de Strasbourg, Institut de Biologie Moléculaire et Cellulaire, 67084 Strasbourg, France

Edited by Thomas A. Steitz, Yale University, New Haven, CT, and approved April 14, 2015 (received for review March 16, 2015)

Elongation factor-catalyzed GTP hydrolysis is a key reaction during the ribosomal elongation cycle. Recent crystal structures of G proteins, such as elongation factor G (EF-G) bound to the ribosome, as well as many biochemical studies, provide evidence that the direct interaction of translational GTPases (trGTPases) with the sarcin-ricin loop (SRL) of ribosomal RNA (rRNA) is pivotal for hydrolysis. However, the precise mechanism remains elusive and is intensively debated. Based on the close proximity of the phosphate oxygen of A2662 of the SRL to the supposedly catalytic histidine of EF-G (His87), we probed this interaction by an atomic mutagenesis approach. We individually replaced either of the two nonbridging phosphate oxygens at A2662 with a methyl group by the introduction of a methylphosphonate instead of the natural phosphate in fully functional, reconstituted bacterial ribosomes. Our major finding was that only one of the two resulting diastereomers, the *S_P* methylphosphonate, was compatible with efficient GTPase activation on EF-G. The same trend was observed for a second trGTPase, namely EF4 (LepA). In addition, we provide evidence that the negative charge of the A2662 phosphate group must be retained for uncompromised activity in GTP hydrolysis. In summary, our data strongly corroborate that the nonbridging *proS_P* phosphate oxygen at the A2662 of the SRL is critically involved in the activation of GTP hydrolysis. A mechanistic scenario is supported in which positioning of the catalytically active, protonated His87 through electrostatic interactions with the A2662 phosphate group and H-bond networks are key features of ribosome-triggered activation of trGTPases.

tRNA translocation | protein biosynthesis | modification | methylphosphonate | RNA solid-phase synthesis

In all three domains of life, translational GTPases (trGTPases), highly conserved members of the G protein family, play diverse and central roles during protein biosynthesis (1–3). G proteins can be regarded as molecular switches that are driven by GTP hydrolysis and cycle between the active GTP-bound state and the inactive GDP-bound form. Although many G proteins require an external GTPase activating protein (GAP) to trigger efficient GTP hydrolysis (4, 5), trGTPases that interact with the ribosome appear to be activated by RNA rather than by a classical GAP (6). In bacteria, ribosome-activated GTPases include the universally present elongation factors (EF)-Tu, EF-G and EF-4 (LepA) and the initiation factor IF2, as well as the less frequently found, yet highly conserved, release factor RF3, tetracycline resistance proteins (TetO), or the selenocysteine incorporation factor SelB (7). Besides the high sequence and structure similarities, trGTPases share the way of association with the large ribosomal subunit, close to the A-site. Biochemical and structural studies identified the sarcin-ricin loop (SRL) of 23S rRNA as one of the most pivotal rRNA elements for trGTPase functioning (8–12). The SRL represents one of the most highly conserved sequences of ribosomal RNA, and its tip has been shown to closely approach the bound GTP molecule in the respective G domains of trGTPases (9, 12). Several lines of evidence highlight the importance of the SRL for effective binding of trGTPases to the ribosome (13, 14). Other studies revealed a

more intricate involvement of the SRL for GTPase activation that goes beyond mere factor binding (14, 15).

The two cytotoxins α-sarcin and ricin cleave or depurinate the SRL at a single site at positions A2662 and A2660, respectively (16). These alterations in the SRL result in a complete block of translation, which is thought to be the consequence of an impaired activation/binding of trGTPases (17). Recent crystal structures of EF-Tu (12), or EF-G (9, 18–21) bound to the ribosome stimulated considerations about the mechanism of ribosome-triggered GTP hydrolysis. Based on the close proximity of the phosphate oxygen at position A2662 of the SRL to the supposedly catalytic histidine of EF-Tu (His84) or EF-G (His87) (Fig. 1*A*), a catalytic model for GTP hydrolysis was proposed (12, 20). In the suggested scenario, the nonbridging oxygen at A2662 positions His84 in its catalytic conformation, thus enabling it to act as a general base by subtracting a proton from the hydrolytic water that attacks the γ-phosphate of GTP (12). This model stimulated an intense scientific discussion in the field (22, 23), because it is not fully compatible with certain biochemical, genetic (24), structural (25), and molecular dynamics simulation (26) data.

To shed light on the possible function of the A2662 phosphate oxygen for activation of trGTPases, we applied here an atomic mutagenesis approach (27). The core of this technique is based on the *in vitro* reconstitution of functional 50S ribosomal

Significance

Translational GTPases are key players in ribosomal protein synthesis. Their intrinsic GTPase activity is low and is stimulated by ribosome association. Although it has been shown by structural and biochemical studies that the sarcin-ricin loop of ribosomal RNA (rRNA) closely approaches the supposedly catalytic His of elongation factor (EF)-G and EF-Tu and thereby may contribute to GTP hydrolysis, the exact mechanism of activation remains unclear and is a matter of controversial debate. Using the atomic mutagenesis approach that allows incorporation of nonnatural 23S rRNA nucleotides into 70S particles, we show that a nonbridging phosphate oxygen of rRNA is key for GTP hydrolysis of translational GTPases. To date, this is only the second rRNA backbone residue shown to be critical in ribosome function.

Author contributions: M.K., S.F., R.M., and N.P. designed research; M.K., S.F., C.K., and E.E. performed research; C.K. and E.E. contributed new reagents/analytic tools; M.K., S.F., C.K., E.E., R.M., and N.P. analyzed data; and M.K., S.F., R.M., and N.P. wrote the paper.

The authors declare no conflict of interest.

This article is a PNAS Direct Submission.

Freely available online through the PNAS open access option.

Data deposition: The atomic coordinates and structure factors have been deposited in the Protein Data Bank, www.pdb.org (PDB ID code 4Y27).

¹M.K. and S.F. contributed equally to this work.

²To whom correspondence may be addressed. Email: ronald.micura@uibk.ac.at or norbert.polacek@dcb.unibe.ch.

This article contains supporting information online at www.pnas.org/lookup/suppl/doi:10.1073/pnas.1505231112/-DCSupplemental.

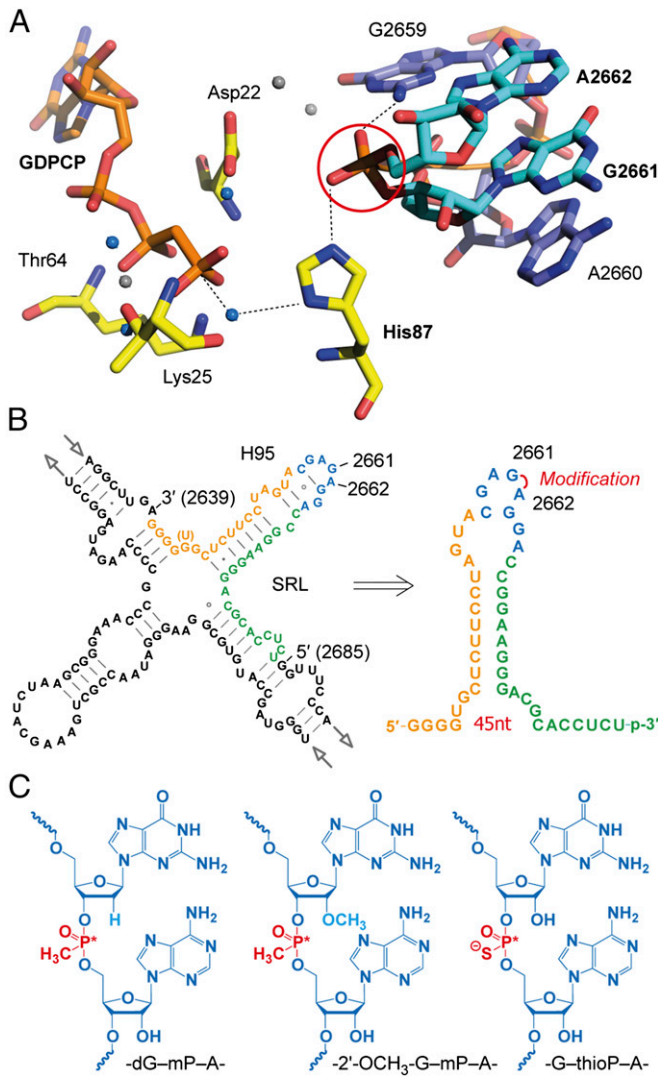


Fig. 1. Catalytic center of ribosome bound EF-G from *Thermus thermophilus* (*T.th.*). (A) Presentation of the catalytic center of EF-G bound to the ribosome. Shown are the GTP analog (GDPCP) and the residues supposed to be required for GTP hydrolysis: Asp22, Thr64, and Lys25 involved in coordination of the catalytic center and GDPCP; A2660–A2662 nucleotides of the SRL; catalytic His87 and its potential interaction with the nonbridging phosphate of A2662 (highlighted by a circle; magenta). Figure is based on the PDB ID codes 4JUW and 4JUX (20). (B) Secondary structure representation of the SRL (H95; 2653–2667) from *T.aq.*; for construction of the ΔSRL mutant, a circularly permuted 23S rRNA was generated by connecting the natural ends in H1 and introducing new end points at positions 2685 (5') and 2639 (3'). To complement the deleted 23S rRNA fragment, a synthetic RNA oligomer (orange-blue-green) was added in *trans* during *in vitro* reconstitution. (C) Modifications investigated at the G2661–A2662 positions to elucidate the role of the crucial backbone phosphate in GTP hydrolysis.

particles of *Thermus aquaticus* (*T.aq.*) from a circularly permuted (cp) 23S rRNA transcript that leaves a sequence gap lacking the SRL segment (Fig. 1*B*). During *in vitro* assembly, this sequence gap is filled with a synthetic RNA oligonucleotide encompassing the SRL region that carries the desired nonnatural nucleotide modification at A2662 (Fig. 1*B*). The atomic mutagenesis approach has previously been successfully applied to study the role of A2660 in the SRL for GTPase activation (15) and elucidated the stringent requirement for the A2660 exocyclic amino group. Here we applied this method for the first time, to our knowledge, to study the role of an rRNA phosphate backbone group in

GTPase activation. We individually replaced either of the two nonbridging phosphate oxygens at A2662 with a methyl group by the introduction of a methylphosphonate instead of the natural phosphate. Our major finding is that only one of the two resulting diastereomers is compatible with efficient GTPase activation on EF-G and EF4 (LepA). Our data strongly corroborate that the nonbridging proS_P phosphate oxygen at the SRL position A2662 is critically involved in the activation of GTP hydrolysis and thereby suggest a profound mechanistic scenario for ribosome-triggered activation of trGTPases.

Results

Chemical Synthesis and Integrity of the A2662 Methylphosphonate-Modified SRL Diastereomers. To address the role of the nonbridging phosphate oxygens of A2662 in activation of EF-G GTP hydrolysis (Fig. 1*A*), we prepared SRL fragments that carried a methylphosphonate at the corresponding position (Fig. 1*B* and *C*).

The replacement of a nonbridging phosphate oxygen by a methyl group was selected, as the latter has no proton acceptor capability and has no lone pair of electrons, thus erasing any possibility for classical hydrogen bond formation (28–33). In addition, by replacing the oxygen through a methyl group, the negative charge at the rRNA backbone at this position is eliminated, which allows investigating the putative role of this charge at A2662 in affecting the acid–base behavior of the conserved His87 and its consequences on GTP hydrolysis.

The methylphosphonate modification generates chirality at the phosphor atom and results in two possible diastereomeric RNAs (*R*_P and *S*_P; Cahn–Ingold–Prelog nomenclature is used throughout the manuscript) (28). Importantly, our experimental design allowed individual access to either of the two diastereomers (Fig. 2). Solid-phase synthesis first provided a diastereomeric mixture of the short 8-nt methylphosphonate oligonucleotide covering the sequence from C2658 to A2655, followed by separation of the two diastereomeric strands using reversed-phase HPLC (Fig. 2*A*). Then, templated enzymatic ligation to achieve the required 45-nt SRL stem-loop segment was conducted with either of the two RNA diastereomers and proceeded in high yields (Fig. 2*B*).

To verify the structural integrity of the methylphosphonate modification that was used in combination with a 2'-deoxy or alternatively a 2'-OCH₃ at G2661 to avoid strand cleavage (31), we performed imino proton ¹H NMR spectroscopy of a corresponding 27-nt SRL RNA, namely 5'-UGC UCC UAG UAC GA(2'-OCH₃-G-mP-A)GG ACC GGA GUG (Fig. 3). Both diastereomers showed nearly identical spectra compared with the WT RNA with the natural phosphodiester moiety (Fig. 3*B*). This observation unequivocally confirmed proper folding into the hairpin in aqueous buffer solution. Additionally, the stereochemical assignment of the two diastereomeric RNAs was tentatively achieved based on nuclear Overhauser enhancement (NOE) patterns observed in a NOESY ¹H, ¹H NMR spectrum (Fig. 3*D*).

To obtain even more detailed structural insights, we put significant efforts into crystallography and indeed succeeded in solving the crystal structure of the 2'-OCH₃-G2661-mP-A2662 *R*_P diastereomer of the 27-nt SRL RNA at 1.0-Å resolution (Fig. 4 and Table S1). The high-resolution structure reveals that the methylphosphonate adopts a similar conformation as observed for the specific phosphate in the natural RNA [RMSD of 0.08 Å with the unmodified isolated SRL (Fig. 4 and Fig. S1) and RMSD of 0.84 Å within the context of the 70S ribosome, PDB 4YBB (34) (Fig. S2)]. The methyl group of the *R*_P methylphosphonate at A2662 is directed outward and coincides with the orientation of the native proS_P nonbridging oxygen.

Taken together, our NMR spectroscopic and X-ray crystallographic analysis provided strong evidence for the structural integrity of the methylphosphonate modification, which represented a fundamental prerequisite for the functional studies described below.

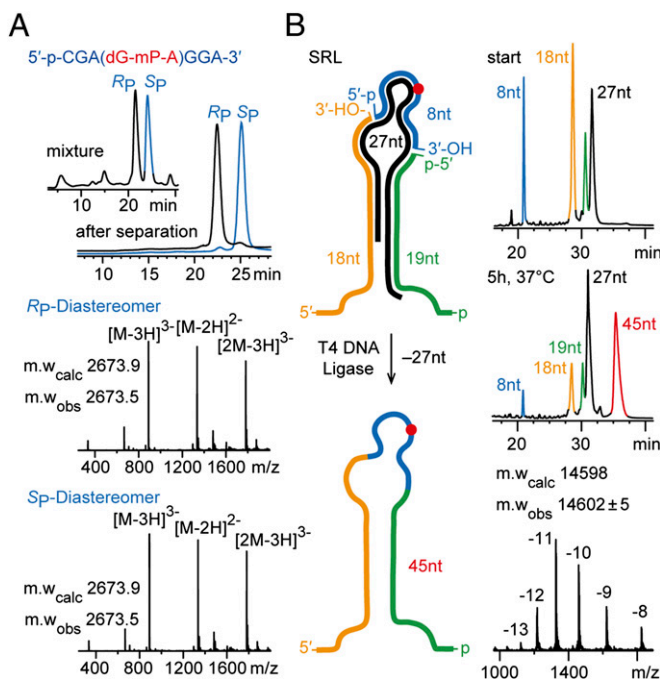


Fig. 2. Synthesis of diastereomerically pure A2662 methylphosphonate modified 45 nt SRL RNA. (A) The crude diastereomeric mixture of the 8nt RNA obtained by solid-phase synthesis was separated by reversed-phase HPLC (Top); corresponding LC-ESI MS analysis (Middle and Bottom). (B) RNA strand setup of the templated enzymatic ligation using T4 DNA ligase (Left), corresponding HPLC traces of a typical ligation experiment, and mass spectrum of the purified 45 nt target RNA (Right), confirming product integrity. RNA sequence: 5'-GGGGUGCUCUUCGUACGA(dG-mP-A)GGACCGGAA-GGGACGCACCUCU-3'.

A2662 Methylphosphonate Does Not Affect Overall 50S Assembly. The synthetic strand was subsequently placed into the 50S ribosomal subunit via the atomic mutagenesis procedure (27). First, we addressed the correct assembly of reconstituted ribosomes, carrying either the WT SRL sequence or one of the methylphosphonate stereoisomers by testing their ability to catalyze peptide bond formation via the puromycin reaction. Results of the puromycin assay showed that both the synthetic SRL fragment carrying the *R_P* and the *S_P* stereoisomer are as active as the WT construct in peptide bond formation (Fig. S3). Because peptide bond formation, a reaction catalyzed by the ribosomal peptidyl transferase center (PTC), proceeds as a single turnover reaction under these conditions (35), one can conclude from these data that comparable amounts of correctly assembled 50S particles were generated in all cases. Globally the 50S ribosomal subunit has to be properly assembled to associate with the native 30S subunit to function in the puromycin assay under the applied conditions. Therefore, we conclude from these data that the methylphosphonate modification at A2662 is well tolerated in the overall assembly of the 50S ribosomal subunit and for 70S association.

Only One A2662 Methylphosphonate Diastereomer (*R_P*) Interferes with GTPase Activation. To test the modified ribosomes for stimulation of EF-G GTP hydrolysis, we performed an uncoupled GTPase assay (15). We used radioactively labeled GTP and followed GTP hydrolysis over time. GTP hydrolysis in the presence of ribosomes lacking the complementing SRL RNA oligonucleotide was considered as background and subtracted from all values. Ribosomes carrying the unmodified (WT) SRL sequence very efficiently stimulated EF-G GTP hydrolysis (Fig. 5). Nearly all GTP, present in the reaction, was hydrolyzed by EF-G

within the first 15 min. Ribosomes carrying the methylphosphonate in the *S_P* configuration were still able to stimulate EF-G GTP hydrolysis, although hydrolysis was reduced compared with the WT control (Fig. 5A). We determined the initial rate of GTP hydrolysis, which was 0.068 s^{-1} and therefore about eightfold reduced compared with reconstituted ribosomes harboring the WT SRL oligo (0.535 s^{-1}). These data are consistent with our structural data of the SRL, indicating that in the *S_P* stereoisomer the methyl group points toward the inside of the SRL loop (Figs. 3A and 4), whereas the remaining nonbridging phosphate oxygen is directed outward and faces the catalytic center of EF-G. It can thus potentially activate the conserved His87. Ribosomes carrying the methylphosphonate in the *R_P* configuration did not stimulate EF-G GTP hydrolysis significantly above background and revealed a drastically 37-fold reduced GTPase rate (Fig. 5A). In our previous study using the same *in vitro* reconstitution construct as here (Fig. 1B), we demonstrated that EF-G binding to *T. aquaticus* ribosomes was not affected by manipulations or ablation of the SRL (15), thus excluding binding defects as cause of the observed differences in EF-G GTPase. These results clearly demonstrate that the nonbridging phosphate oxygen of A2662 in the pro*S_P* configuration plays a critical role in stimulating EF-G GTP hydrolysis.

As it was proposed that the mechanism of GTPase stimulation by the ribosome and GTP hydrolysis is conserved for all trGTPases (12), we tested ribosomes carrying the methylphosphonate modification for their ability to stimulate GTP hydrolysis of EF4 (LepA). The overall GTPase activity of EF4 in our assay was markedly lower, about fourfold reduced, compared with EF-G. In accordance with the EF-G data above, essentially no EF4 GTP hydrolysis was observed in the presence of ribosomes carrying the *R_P* stereoisomer of the methylphosphonate analog at A2662 (0.001 s^{-1}) (Fig. 5B).

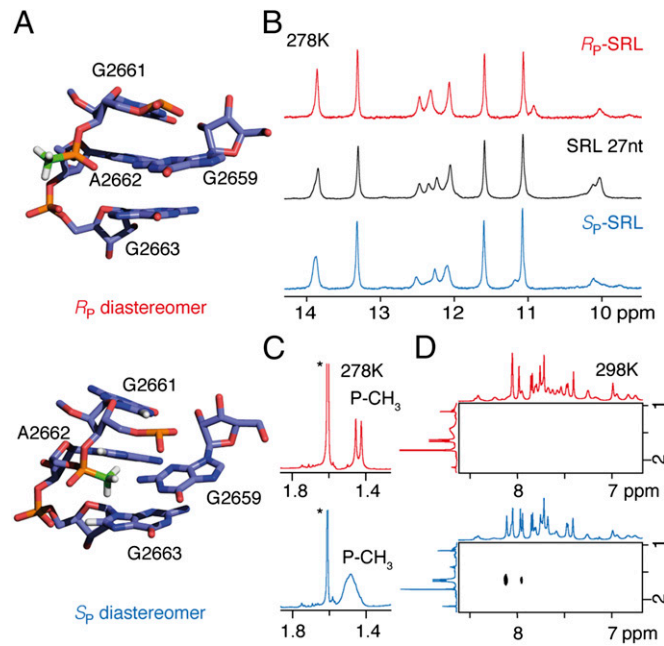


Fig. 3. NMR spectroscopic analysis of G2661-A2662 methylphosphonate modified 27 nt SRL RNA. (A) 3D model of the two diastereomers based on PDB ID code 4Y27. (B) Comparison of imino proton ^1H NMR spectra confirm structural integrity of stem-loop formation in solution. (C) ^1H NMR spectra indicate slightly hindered methyl group rotation for the *S_P* diastereomer. (D) Diasteromeric assignment was based on ^1H , ^1H NOESY spectroscopy showing cross-peaks of the *S_P* methyl group and aromatic nucleobase protons. RNA sequence: 5'-UGCUCCUAGUACGA(2'-OCH₃-G-mP-A)GGACCGGAGUG-3'. For conditions, see Materials and Methods.

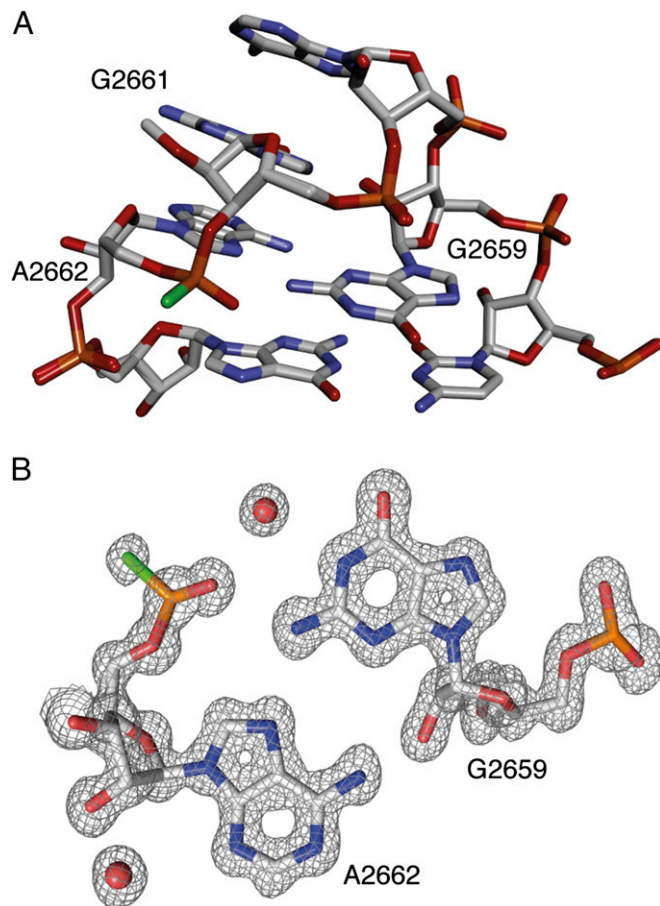


Fig. 4. X-ray structure of a G2661–A2662 methylphosphonate-modified 27 nt SRL RNA at 1.0-Å resolution. (A) Overlay of modified and unmodified (53) RNA (PDB ID codes 4Y27 and 3DVZ) shows that the two structures are nearly identical, and also at the site of modification (RMSD, 0.08 Å). The R_P methylphosphonate at A2662 is shown in green. (B) The 2Fo-Fc electron density map is shown contoured at the 1.0 σ level around residues G2659 and A2662, clearly showing the density corresponding to the methylphosphonate modification on the latter residue. Two surrounding water molecules are depicted with red spheres. RNA sequence: 5'-UGCUCCUAGUACGA (2'-OCH₃-G-mP-A)GGA-CCGGAGUG-3'.

On the other hand, the S_P diastereomer was able to trigger EF4 GTPase, albeit to a lesser degree than the unmodified WT SRL fragment (Fig. 5B).

In sum, these results demonstrate that the nonbridging phosphate oxygen in the pro S_P configuration that points toward the key GTPase residue His87 (see refs. 12 and 20 and our own structural data, Figs. 3A and 4) is essential for stimulation of GTP hydrolysis by EF-G and EF4.

A2662 Thiophosphate Diastereomers Both Have WT Activities in GTPase Hydrolysis. For an additional reference experiment, we substituted the nonbridging oxygens of the original phosphate at position A2662 by sulfur atoms (Fig. 1C, Right). SRL strands with both thiophosphate configurations were individually synthesized using the same strategy as elaborated for the methylphosphonates described above (Fig. 2). Subsequently, these RNAs were incorporated into the 50S ribosomal subunit. Like a phosphodiester group in the RNA backbone, the thiophosphate analog is charged, and therefore, its chemical properties are much closer to the original phosphate compared with the methylphosphonate. Its pK_a value is estimated to be decreased by only about one unit [compare, for example, HSPO₃²⁻ pK_a 5.5 and

HPO₄²⁻ pK_a 6.8 (36); or GMP pK_a 6.2 and GMPS pK_a 5.0 (37)] and thus, it is not surprising that the thiophosphate analog of A2662 was active in the EF-G GTPase assay (Fig. 6A and Fig. S4A). More precisely, both thiophosphate diastereomers could stimulate GTP hydrolysis as efficiently as the WT control. These data support the conclusion that the negative charge of the backbone moiety between SRL G2661 and A2662 represents a crucial determinant in the mechanistic scenario of GTPase activation.

Elimination of the Negative Charge at the A2662 Renders GTP Hydrolysis pH Dependent. It has been shown before that GTP hydrolysis by EF-Tu is pH independent (in the range between pH 6.5 and 8.5) and therefore a primary role of His84 (EF-Tu) as a general base in GTP hydrolysis was excluded (24). However, molecular simulation experiments lead to the suggestion that removal of the negative charge at the phosphate backbone at position A2662 would render the reaction pH dependent (38). Consequently, we decided to test ribosomes carrying the methylphosphonate in the S_P configuration in activation of EF-G GTP hydrolysis at different pH values between 7.4 and 6.0. In parallel, we tested ribosomes carrying the WT SRL sequence, for which we expected pH independence as demonstrated previously for EF-Tu and ribosomes composed of natural 50S (24). It has been shown previously that within this pH range both the elongation factor and the ribosome stay intact (39, 40). In our hands, reconstituted ribosomes harboring the WT SRL fragment efficiently stimulated EF-G GTP hydrolysis at all pH tested; only at the lowest pH 6.0 did we observe a slight decrease in the reaction rate (Fig. 6B and Fig. S4B). Modified ribosomes containing a methylphosphonate in the S_P configuration at position A2662, however, did not efficiently stimulate GTP hydrolysis at lower pH values, and the relative reaction rates dropped markedly compared with the WT control (Fig. 6B). Thus, substituting the nonbridging oxygen by a methyl group and concomitantly eliminating the negative charge

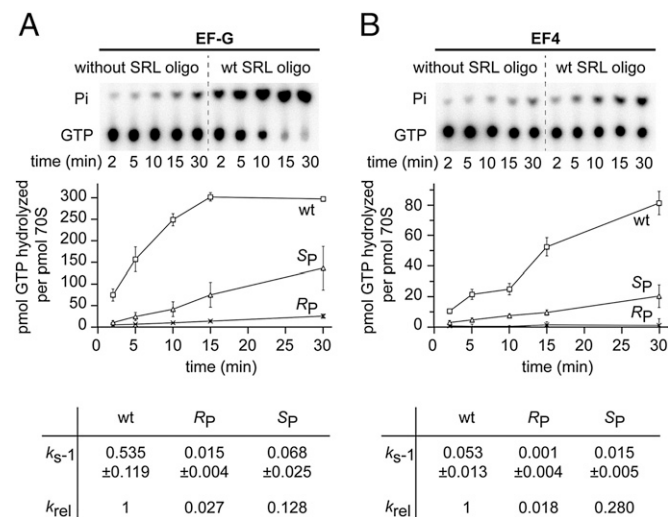


Fig. 5. Uncoupled EF-G GTPase activities using reconstituted ribosomes with the A2662 methylphosphonate SRL modification. (A) Representative time course of ribosome-dependent uncoupled EF-G GTP hydrolysis, using reconstituted ribosomes (without or with WT complementing RNA oligomer). (Top) Products were separated via TLC and visualized by phosphor imaging. GTP hydrolysis was quantified using Aida image analysis software. (Middle) Means and the SD of three independent experiments. Rates of GTP hydrolysis [$k(s^{-1})$] were calculated from the first three time points, for relative GTP hydrolysis rates (k_{rel}). WT hydrolysis rate was set to 1 (Bottom). (B) Uncoupled EF4 GTPase activity stimulated by reconstituted ribosomes. Experiments and analysis were performed as described above for EF-G. Modified SRL oligomers contained the 2'-OCH₃-G2661-mP-A2662 unit.

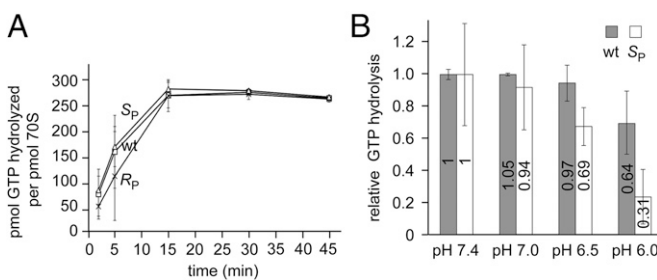


Fig. 6. Impact of A2662 thiophosphate SRL (A) and pH dependence of A2662 *S_P* methylphosphonate SRL (B) on EF-G GTP hydrolysis rates. (A) Uncoupled EF-G GTPase activities using reconstituted ribosomes with the thiophosphate SRL modification. Both diastereomers (*R_P* and *S_P*) possess WT activities. (B) For uncoupled ribosome-stimulated EF-G GTP hydrolysis, 2 pmol reconstituted ribosomes (WT and *S_P* methylphosphonate) were incubated with 15 pmol EF-G and 670 pmol GTP at different pH (7.4, 7.0, 6.5, and 6.0). Products were separated via TLC and visualized by phosphor imaging. GTP hydrolysis was quantified using Aida image analysis software. Quantification shows the relative GTP hydrolysis after 30 min of incubation. GTP hydrolysis at standard pH, pH 7.4, was set to 1. Means and SD of three independent experiments are shown. Relative rates (k_{rel}) of GTP hydrolysis are indicated within the bars.

at A2662 renders the EF-G promoted GTP hydrolysis reaction pH sensitive.

Discussion

trGTPases possess low intrinsic GTP hydrolysis activity, which is, however, substantially stimulated by ribosome association, suggesting that a part of the ribosome is involved in catalysis or in some conformational arrangements in the trGTPases required for GTP hydrolysis. It has been shown by structural and biochemical data that residues G2655, A2660, G2661, and A2662 (9, 10, 12) of the SRL are involved in binding of EF-Tu or EF-G to the ribosome, suggesting they may also contribute to GTPase activation. Using the atomic mutagenesis approach, the nucleobase exocyclic amino group of A2660 was identified as critical for EF-G GTPase activation; however, the exact contribution of this residue remained unclear (15). One possible scenario is that it contributes to the correct arrangement of the catalytic center of trGTPases by stacking interactions, which is emphasized by a recent crystal structure of EF-G on the ribosome, where A2660 was suggested to stack on Arg660 of EF-G (18).

Another residue of the 23S rRNA, which was proposed to be involved in GTPase activation, is the nonbridging phosphate oxygen of A2662. Based on the structure of EF-Tu on the ribosome, Vorhees et al. suggested a mechanism for GTP hydrolysis. In this model, His84 acts as a general base catalyst and is activated by the phosphate oxygen of A2662 (12). However, as GTP hydrolysis is pH independent, one may exclude that His84 functions as a general base catalyst (24). Furthermore, the fact that the conserved histidine is surrounded by several negative charges indicates its pK_a to be elevated and thus its side chain to be protonated at physiological pH (41). Nevertheless, the proposed general base mechanism continues to be intensively discussed and the role of the SRL, and the conserved histidine remains unclear (22, 23). Recent studies favor a model where GTP hydrolysis is activated via substrate-assisted catalysis, thereby highlighting the importance of functional groups on the GTP substrate for the phosphoryl transfer mechanism (41, 42). However, the contribution of the nonbridging phosphate oxygen at position 2662 of rRNA to GTP hydrolysis is still unclear.

Here we addressed this open point by using the atomic mutagenesis approach to site specifically modify the phosphate backbone of the rRNA. Thereby, we demonstrated that one of the nonbridging phosphate oxygen (pro*S_P*) at A2662 is involved in activation of EF-G GTP hydrolysis, as its replacement with a

methyl group results in ribosomes severely hampered in triggering EF-G GTPase (Fig. 5). On the other hand, ribosomes harboring the *S_P* diastereomer of the methylphosphonate-modified SRL, which renders the residual nonbridging oxygen in proper orientation, directed toward the crucial histidine (Fig. 3), still possess substantial activity in triggering GTP hydrolysis. This observation is evidence that the mere introduction of a methyl group at this position of the SRL does not globally disrupt rRNA architecture (Fig. 4A and Fig. S1); thus, the observed effects with the two diastereomers can be considered as specific. Nevertheless, the active stereoisomer (*S_P*) did not stimulate EF-G GTPase hydrolysis as efficiently as ribosomes carrying a regular phosphodiester bridge between positions G2661 and A2662. It is possible that replacing the nonbridging pro*R_P* oxygen by the more bulky methyl group renders the SRL structure less compact. In any case, this replacement unsets one original hydrogen bond, between the pro*R_P* oxygen and the exocyclic amino group of G2659. Also, the NMR spectra indicated that rotation of the methyl group (*S_P* diastereomer) is slightly hindered at low temperature (Fig. 3C, Lower) compared with rotation of the methyl group of the corresponding *R_P* diastereomer (Fig. 3C, Upper). Thus, it cannot be completely excluded that introducing a methyl group in the *S_P* configuration may slightly affect the functionally competent loop conformation for efficiently triggering GTP hydrolysis.

A more likely and favored explanation for the reactive, but eightfold reduced, activity of the *S_P* configurated methylphosphonate is the following: the introduction of the methyl group instead of the nonbridging oxygen removes a negative charge at the A2662 backbone. This charge, however, is substantial for the interaction with His87, enabling the formation of a very strong hydrogen bond. Removing the charge at the nonbridging oxygen (*S_P* diastereomer) is consistent with weakening these interactions and hence reducing activity for GTP hydrolysis. Likewise, total replacement of the nonbridging oxygen by a methyl group (*R_P* diastereomer) is consistent with abrogating these interactions and consequently abolishing substrate hydrolysis.

The negative charge of the phosphate may contribute to increase the pK_a of the catalytic histidine and thus enable protonation

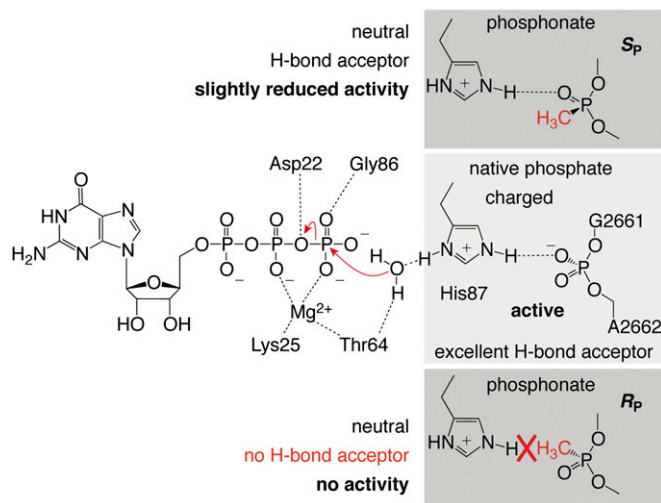


Fig. 7. Model for EF-G-triggered GTP hydrolysis at the ribosome. The native, charged phosphate of A2662 assists in positioning of His87 (Middle). The *S_P* methylphosphonate is available for hydrogen bonding to His87 but is uncharged, and hence, the activity is slightly reduced (Top). The *R_P* methylphosphonate impairs positioning of His87, and hence, no activity is observed (Bottom). This interpretation is consistent with the observation that the corresponding A2662 phosphorothioate diastereomers—that are both charged and available for electrostatic interactions and H-bond networks—represent reactive probes; they provide activities that are comparable to WT.

of the imidazole nitrogen as previously proposed by computer simulations (41). The protonated histidine could then donate this proton to form a hydrogen bond to the catalytic water. In this scenario, the water is then ideally positioned in a way that allows the γ -phosphate of GTP to subtract a water proton. This substrate-generated hydroxide ion subsequently attacks the γ -phosphate, leading to GTP hydrolysis (Fig. 7). In the A2662 methylphosphonate-modified ribosomes, the active S_P stereoisomer is still able to hydrogen bond to the active site histidine; however, due to the absence of the negative charge at the SRL backbone, the pK_a shift at the catalytic histidine appears not to be as substantial as in ribosomes carrying a phosphodiester bond (Fig. 7). This catalytic scenario and the significance of the negative charge at A2662 are compatible with the phosphorothioate-modified SRL, because both stereoisomers carry a negative charge and trigger GTPase as efficiently as the WT control (Fig. 6).

This mechanistic model is also compatible with recent *in silico* approaches that predict the catalytic histidine (His84 of *Escherichia coli* EF-Tu) to be protonated and to be part of an allosteric repositioning of active site residues (38). The authors suggest that for such an allosteric model, the electrostatic interaction between the positively charged histidine and the negatively charged phosphate oxygen at A2662 is important, and they predict that the removal of the latter charge would render GTP hydrolysis pH dependent. Our data are fully compatible with this prediction because the elimination of the negative charge at A2662 results in a GTP hydrolysis reaction that is inhibited at low pH values compared with the WT control (Fig. 6).

Although our data contribute to the understanding of the role of the nonbridging phosphate oxygen at A2662 of the SRL for ribosome-triggered GTP hydrolysis, it does not yet allow a complete mechanistic model to be drawn. Very recently another residue, namely an aspartate residue (Asp21 of EF-Tu), has been shown to be crucial for stimulation of GTP hydrolysis by EF-Tu on cognate decoding, whereas it is dispensable for intrinsic GTPase activity (42). It was suggested that basal GTP hydrolysis of trGTPases does not involve side chains of Asp21 and His84. This consideration further raises the intriguing possibility that the mechanism of GTP hydrolysis differs on and off the ribosome.

In this work, we could show that the pro S_P nonbridging phosphate oxygen of A2662 is required for stimulating GTPase activity of the two trGTPases EF-G and EF4. This specific phosphate is only the second example for an rRNA backbone functional group that has been identified thus far using the atomic mutagenesis technique to play a pivotal role in ribosomal reactions. Although for ribosome-catalyzed peptide bond formation, the ribose 2'-OH at A2451 has been shown to be important (35, 43–45), here we demonstrate the nonbridging phosphate oxygen of A2662 to participate in activating GTP hydrolysis on trGTPases.

Materials and Methods

RNA Methylphosphonate Synthesis. Standard phosphoramidite chemistry was applied for RNA strand elongation and incorporation of methylphosphonates (46). 2'-O-TOM standard RNA nucleoside phosphoramidites were purchased from ChemGenes, dG and 2'-OCH₃-G methyl phosphonamidites from ChemGenes and Glen Research, and polystyrene support from GE Healthcare (Custom Primer Support, 80 μ mol/g; PS 200). All oligonucleotides were synthesized on a ABI 392 Nucleic Acid Synthesizer following standard methods: detritylation (80 s) with dichloroacetic acid/1,2-dichloroethane (4/96); coupling (2 min for standard amidites and 6 min for methylphosphonamidites) with phosphoramidites/acetonitrile (0.1 M \times 130 μ L) and benzylthiotetrazole/acetonitrile (0.3 M \times 360 μ L); capping (3 \times 0.4 min, Cap A/Cap B = 1/1) with Cap A: 4-(dimethylamino)pyridine in acetonitrile (0.5 M) and Cap B: Ac₂O/sym-collidine/acetonitrile (2/3/5); and oxidation (1.0 min) with I₂ (20 mM) in tetrahydrofuran (THF)/pyridine/H₂O (35/10/5). The solutions of amidites and tetrazole in acetonitrile were dried over activated molecular sieves (4 \AA) overnight. Although 2'-deoxy-5'-O-(4,4'-dimethoxytrityl)-N²-isobutyryl-guanosine 3'-(methyl-(N,N-diisopropyl))-phosphonamidite had to be dis-

solved in tetrahydrofuran, the corresponding 2'-OCH₃-G phosphonamidite was applied in acetonitrile.

RNA Thiophosphate Synthesis. For the synthesis of thiophosphate-containing RNA, automated phosphoramidite chemistry was applied as described above. Sulfur was introduced manually using phenylacetyl disulfide (PADS) in analogy to ref. 47.

Deprotection of Methylphosphonate-Modified RNA. The solid support was treated with 0.5 mL of a mixture of concentrated aqueous ammonium hydroxide solution/ethanol/acetonitrile [10/45/45 (vol/vol/vol)] for 30 min at room temperature. Then, 0.5 mL ethylenediamine was added, and the mixture was agitated or 5 h at room temperature. The supernatant was filtered into a 100-mL round-bottomed flask, and the solid support was washed twice with ethanol/water [1/1 (vol/vol)]. The supernatant and the washings were combined, and triethylammonium bicarbonate (TEAB) (1 M, 1 mL) was added. The solution was evaporated, and a clear oil was obtained. To remove the 2'-silyl protecting groups, the resulting oil was treated with tetrabutylammonium fluoride trihydrate (TBAF-3 H₂O) in THF (1 M, 1 mL), and the suspension was agitated at 37 °C overnight. The reaction was quenched by the addition of triethylammonium acetate (TEAA) (1 M, pH 7.4, 1 mL). The volume of the solution was reduced, and the solution was desalting with a size exclusion column (GE Healthcare, HiPrep 26/10 Desalting; 2.6 \times 10 cm; Sephadex G25) eluting with H₂O, and the collected fraction was evaporated to dryness and dissolved in 1 mL H₂O. Analysis of the crude RNA after deprotection was performed by anion-exchange chromatography on a Dionex DNAPac PA-100 column (4 \times 250 mm) at 80 °C. Flow rate, 1 mL/min; eluent A, 25 mM Tris-HCl (pH 8.0), 6 M urea; eluent B, 25 mM Tris-HCl (pH 8.0), 0.5 M NaClO₄, 6 M urea; gradient, 0–60% B in A within 45 min or 0–40% B in 30 min for short sequences up to 15 nucleotides; UV detection, 260 nm.

Deprotection of Thiophosphate-Modified RNA. Deprotection was conducted as for unmodified RNA following standard procedures described in ref. 48.

Purification of the Methylphosphonate- and Thiophosphate-Modified RNA. Crude RNA products were purified on a semipreparative Dionex DNAPac PA-100 column (9 \times 250 mm) at 80 °C with a flow rate of 2 mL/min. Fractions containing RNA were loaded on a C18 SepPak Plus cartridge (Waters/Millipore), washed with 0.1–0.15 M (Et₃NH)⁺HCO₃⁻, H₂O, and eluted with H₂O/CH₃CN (1/1). RNA-containing fractions were lyophilized. Analysis of the quality of purified RNA was performed by anion-exchange chromatography with the same conditions as for crude RNA; the molecular weight was confirmed by LC-electrospray ionization (ESI) MS. Yield determination was performed by UV photometrical analysis of oligonucleotide solutions.

Separation of Methylphosphonate- and Thiophosphate-Containing RNA Diastereomers. RNA diastereomers were separated on a reversed-phase GE Healthcare Resource RPC (3 mL; 6.4 \times 100 mm) column at 40 °C with a flow rate of 2 mL/min; elutant A, 0.1 M ammonium acetate, pH 7.0; elutant B, acetonitrile (HPLC grade); gradient, 0–4% B in A within 45 min for sequences up to 30 nucleotides; UV detection, 260 nm. Fractions containing RNA were loaded on a C18 SepPak Plus cartridge (Waters/Millipore), washed with 0.1–0.15 M (Et₃NH)⁺HCO₃⁻, H₂O, and eluted with H₂O/CH₃CN (1/1). RNA-containing fractions were evaporated, and the residue was dissolved in H₂O and lyophilized. Analysis of the RNA diastereomers after separation was performed by reverse-phase chromatography on a XBridge C18 column (130 Å, 5.0 μ m, 4.6 \times 150 mm) at 40 °C. Flow rate, 1 mL/min; elutant A, 0.1 M ammonium acetate, pH 7.0; elutant B, acetonitrile (HPLC grade); gradient, 3–5% B in A within 25 min; UV detection, 260 nm. SRL methylphosphonate stereochemistry was assigned by NMR spectroscopy (Fig. 3); SRL thiophosphate stereochemistry was tentatively assigned based on their retention time by reversed-phase column chromatography according to ref. 49.

Enzymatic Ligation of Diastereomerically Pure Methylphosphonate- and Thiophosphate-Containing RNA. Enzymatic ligation experiments using T4 DNA ligase (Fig. 2) were performed with the separated RNA diastereomers in analogy to a previously published procedure (50).

MS of Modified RNA. All experiments were performed on Finnigan LCQ Advantage MAX ion trap instrumentation connected to an Amersham Etan micro LC system. RNA sequences were analyzed in the negative-ion mode with a potential of –4 kV applied to the spray needle. LC: sample (200 pmol RNA dissolved in 30 μ L of 20 mM EDTA solution; average injection volume: 30 μ L); column (Waters XTerraMS, C18 2.5 μ m; 1.0 \times 50 mm) at 21 °C; flow rate, 30 μ L/min; elutant A,

8.6 mM TEA, 100 mM 1,1,1,3,3-hexafluoroisopropanol in H₂O (pH 8.0); eluant B, methanol; gradient, 0–100% B in A within 30 min; UV detection, 254 nm.

NMR Spectroscopy. The RNA sample was lyophilized and dissolved in D₂O containing 10 mM KH₂PO₄ and 50 mM KCl, pH 6.4. The final RNA concentration was 0.2 mM. The ¹H 1D-NMR spectra were acquired using a double-pulsed field gradient spin-echo pulse sequence.

The NOESY ¹H, ¹H-NMR spectra were acquired on a Bruker Avance II+ 600 MHz spectrometer equipped with a proton-optimized triple resonance NMR ‘inverse’ probe (TCI) CryoProbe Prodigy (5 mm). The NOESY spectra were acquired at 278 or 298 K (Fig. 3). The size of the data matrices were 2,048 × 300 complex data points, the number of scans was 144, the interscan delay was 1.5 s, and the mixing time was set to 150 ms, resulting in a total measuring time of 20 h for each spectrum.

X-Ray Crystallography. The 27-nt SRL hairpin modified with methylphosphonate at the G2661–A2662 step and a 2'-OCH₃ group on the G2661 residue was chemically synthesized. The diastereomers were separated by reversed-phase column chromatography, and the R_P diastereomer was used for crystallization. RNA was dissolved in a buffer made with 1 mM Na EDTA, pH 8.0, and 10 mM Tris-HCl, pH 8.0, at a 350 μM concentration. The RNA sample was heated at 55 °C for 10 min and cooled at 25 °C by switching off the heating block. Crystals were grown for 2 wk at 20 °C by mixing one volume of the RNA sample with one volume of a crystallization buffer made with 2.5 M ammonium sulfate, 10 mM magnesium acetate, and 50 mM 2-(N-morpholino)ethanesulfonic acid (Mes), pH 5.6. Crystals were cryoprotected for about 5 min in a reservoir solution containing 15% (vol/vol) glycerol and 3.0 M ammonium sulfate and flash-frozen in liquid ethane for data collection. X-ray diffraction data were collected using a fine slicing strategy (0.2° oscillation) using the x06SA beamline at the SLS synchrotron (51). Data were processed with the XDS Package (52). The structure was solved by molecular replacement using an unmodified SRL structure as a search model [Protein Data Bank (PDB) ID code 3DVZ] (53) and MOLREP (54) and refined with the PHENIX package (55). The model was built using Coot (56).

Reconstitution of 50S Subunits. Generation of the circularly permuted (cp) 23S rRNA, subsequent in vitro reconstitution of the 50S particles, and reassociation with native 30S subunits were done as previously described (15, 27, 43).

The plasmid pUC19-cp2685-2639, encoding the cp2685-2639 rRNA under the control of the T7 promoter, was linearized using NsiI. The linearized plasmid was used as template for in vitro transcription. For generation of pUC19-cp2685-2639, the 23S was PCR amplified from pCPTaq23S (35) using the following primer: EcoRI-T7-2585 5'-CCGAATTCGGATCTAAATCGACTCACTATAGGTTCC-CAGCTGTCCCTCAGGGGCATA-3' and HindIII-NsiI-Taq2639 5'-CCCCAAGCT-

TATGCATCAAGCCTCTGGCCCGT-3'. The purified PCR product was cloned into pUC19 via the EcoRI and HindIII restriction sites.

To compensate the missing RNA sequence in the cp-23S rRNA, the following RNA oligos were added during in vitro reconstitution: 2640–2684 5'-GGGGUGUCUUCUAGUACGA-G2661-A2662-GGACCGGAAGGGACGCCUCU-3', with the following modifications—dG2661-mP-A2662 (both diastereomers); 2'-OCH₃-G2661-mP-A2662 (both stereoisomers); and G2661-thioP-A2662 (both stereoisomers); for control experiments—dG2661; 2'-OCH₃-G2661. The G2644U mutation is used to facilitate SRL strand annealing to cp-23S rRNA.

Puromycin Reaction. The peptidyl transferase assay was carried out as previously described in ref. 35 using 1 pmol *N*-acetyl-[³H]-Phe-tRNA^{Ph}e (15,000 cpm/pmol) as P-site substrate and 2 mM puromycin as acceptor substrate.

Multiple-Turnover EF-G GTP Hydrolysis. For the uncoupled GTP hydrolysis assay, reconstituted ribosomes (20 pmol cp2685-2639 23S rRNA, 200 pmol RNA oligo 2640–2684, and 2 pmol 30S *E.coli*) were ethanol precipitated for 30 min at –80 °C and centrifuged for 20 min at 18,000 × g at 4 °C, and the ribosomal pellet was resuspended in 5 μL GTPase reaction buffer (10.4 mM Tris-HCl, pH 7.4, 208 mM NH₄Cl, 7.8 mM MgCl₂, 0.1 mM EDTA, 3.12 mM spermidine, and 2.6 mM 2-mercaptoethanol). The following reaction was performed in GTPase reaction buffer: 0.7 μM deacylated tRNA^{Ph}e was bound to the P-site of reconstituted ribosomes in the presence of 26 μg poly(U) for 5 min at 37 °C. The reaction was initiated by addition of 50 μM (γ -³²P)GTP (6,000 Ci/mmol, 10 mCi/mL; Perkin Elmer) and 1.14 μM his-tagged EF-G from *Thermus thermophilus* in a total volume of 13.4 μL and incubated at 37 °C. At the indicated time points, 2 μL was withdrawn from the reaction and terminated by the addition of one volume of 20% (vol/vol) formic acid. Hydrolysis products were separated by TLC in 0.5 M KH₂PO₄ as the solvent system (15). TLC (Polygram CEL300 PEI/UV) plates were dried, exposed for 1–2 h, and scanned at the phosphorimager (FujiFilm). GTP hydrolysis in the absence of any complementing RNA oligonucleotide was considered as background, coming from slight contaminations of the 30S with native 50S and was subtracted from all experimental points. For the pH dependency assay, reactions were performed as described above; however, GTPase reaction buffer contained 10.4 mM Tris-HCl, pH 7.0, 6.5, and 6.0.

ACKNOWLEDGMENTS. We thank Cyrielle Da Veiga for crystallization and Dr. Vincent Olieric for assistance in data collection. This research was partly supported by the National Centers of Competence in Research (NCCR) “RNA & Disease” funded by the Swiss National Science Foundation and Swiss National Science Foundation Grant 31003A_143388/1 (to N.P.). Funding by Austrian Science Foundation Fonds zur Förderung der wissenschaftlichen Forschung (FWF) Grants I1040 (to R.M.) and I844 and P26550 (to C.K.) is acknowledged.

1. Achenbach J, Nierhaus KH (2014) The mechanics of ribosomal translocation. *Biochimie*, in press.
2. Byryzakov Z, Vesper O, Moll I (2013) Ribosome heterogeneity: Another level of complexity in bacterial translation regulation. *Curr Opin Microbiol* 16(2):133–139.
3. Starosta AL, Lassak J, Jung K, Wilson DN (2014) The bacterial translation stress response. *FEMS Microbiol Rev* 38(6):1172–1201.
4. Scheffzek K, et al. (1997) The Ras-RasGAP complex: Structural basis for GTPase activation and its loss in oncogenic Ras mutants. *Science* 277(5324):333–338.
5. Wittinghofer A, Scheffzek K, Ahmadian MR (1997) The interaction of Ras with GTPase-activating proteins. *FEBS Lett* 410(1):63–67.
6. Clementi N, Polacek N (2010) Ribosome-associated GTPases: The role of RNA for GTPase activation. *RNA Biol* 7(5):521–527.
7. Margus T, Remm M, Tenson T (2007) Phylogenetic distribution of translational GTPases in bacteria. *BMC Genomics* 8:15.
8. Connell SR, et al. (2007) Structural basis for interaction of the ribosome with the switch regions of GTP-bound elongation factors. *Mol Cell* 25(5):751–764.
9. Gao YG, et al. (2009) The structure of the ribosome with elongation factor G trapped in the posttranslational state. *Science* 326(5953):694–699.
10. Moazed D, Robertson JM, Noller HF (1988) Interaction of elongation factors EF-G and EF-Tu with a conserved loop in 23S RNA. *Nature* 334(6180):362–364.
11. Villa E, et al. (2009) Ribosome-induced changes in elongation factor Tu conformation control GTP hydrolysis. *Proc Natl Acad Sci USA* 106(4):1063–1068.
12. Voorhees RM, Schmeing TM, Kelley AC, Ramakrishnan V (2010) The mechanism for activation of GTP hydrolysis on the ribosome. *Science* 330(6005):835–838.
13. Mitkevich VA, et al. (2012) GTPases IF2 and EF-G bind GDP and the SRL RNA in a mutually exclusive manner. *Sci Rep* 2:843.
14. Shi X, Khade PK, Sanbonmatsu KY, Joseph S (2012) Functional role of the sarcin-ricin loop of the 23S rRNA in the elongation cycle of protein synthesis. *J Mol Biol* 419(3–4):125–138.
15. Clementi N, Chirkova A, Puffer B, Micura R, Polacek N (2010) Atomic mutagenesis reveals A2660 of 23S ribosomal RNA as key to EF-G GTPase activation. *Nat Chem Biol* 6(5):344–351.
16. Macbeth MR, Wool IG (1999) Characterization of in vitro and in vivo mutations in non-conserved nucleotides in the ribosomal RNA recognition domain for the ribotoxins ricin and sарcіn and the translation elongation factors. *J Mol Biol* 285(2):567–580.
17. García-Ortega L, Alvarez-García E, Gavilanes JG, Martínez-del-Pozo A, Joseph S (2010) Cleavage of the sarcin-ricin loop of 23S rRNA differentially affects EF-G and EF-Tu binding. *Nucleic Acids Res* 38(12):4108–4119.
18. Chen Y, Feng S, Kumar V, Ero R, Gao YG (2013) Structure of EF-G-ribosome complex in a pretranslocation state. *Nat Struct Mol Biol* 20(9):1077–1084.
19. Pulk A, Cate JH (2013) Control of ribosomal subunit rotation by elongation factor G. *Science* 340(6140):1235970.
20. Tourigny DS, Fernández IS, Kelley AC, Ramakrishnan V (2013) Elongation factor G bound to the ribosome in an intermediate state of translocation. *Science* 340(6140):1235490.
21. Lin J, Gagnon MG, Bulkley D, Steitz TA (2015) Conformational changes of elongation factor G on the ribosome during tRNA translocation. *Cell* 160(1–2):219–227.
22. Liljas A, Ehrenberg M, Åqvist J (2011) Comment on “The mechanism for activation of GTP hydrolysis on the ribosome”. *Science* 333(6038):37, author reply 37.
23. Voorhees RMS, Schmeing TM, Kelley AC, Ramakrishnan V (2011) Response to comment on “The mechanism for activation of GTP hydrolysis on the ribosome.” *Science* 333(6038):37b.
24. Daviter T, Wieden HJ, Rodnina MV (2003) Essential role of histidine 84 in elongation factor Tu for the chemical step of GTP hydrolysis on the ribosome. *J Mol Biol* 332(3):689–699.
25. Zhou J, Lancaster L, Trakhanov S, Noller HF (2012) Crystal structure of release factor RF3 trapped in the GTP state on a rotated conformation of the ribosome. *RNA* 18(2):230–240.
26. Åqvist J, Lind C, Sund J, Wallin G (2012) Bridging the gap between ribosome structure and biochemistry by mechanistic computations. *Curr Opin Struct Biol* 22(6):815–823.
27. Erlacher MD, Chirkova A, Voegeli P, Polacek N (2011) Generation of chemically engineered ribosomes for atomic mutagenesis studies on protein biosynthesis. *Nat Protoc* 6(5):580–592.

- PNAS
28. Lischner T, Engels JW (1990) Diastereomeric dinucleoside-methylphosphonates: Determination of configuration with the 2-D NMR ROESY technique. *Nucleic Acids Res* 18(17):5083–5088.
29. Reynolds MA, et al. (1996) Synthesis and thermodynamics of oligonucleotides containing chirally pure R(P) methylphosphonate linkages. *Nucleic Acids Res* 24(22): 4584–4591.
30. Hamma T, Miller PS (2003) Interactions of hairpin oligo-2'-O-methylribonucleotides containing methylphosphonate linkages with HIV TAR RNA. *Antisense Nucleic Acid Drug Dev* 13(1):19–30.
31. Pritchard CE, et al. (1994) Methylphosphonate mapping of phosphate contacts critical for RNA recognition by the human immunodeficiency virus tat and rev proteins. *Nucleic Acids Res* 22(13):2592–2600.
32. Mujeeb A, Reynolds MA, James TL (1997) High-resolution NMR of an antisense DNA x RNA hybrid containing alternating chirally pure Rp methylphosphonates in the DNA backbone. *Biochemistry* 36(9):2371–2379.
33. Dertinger D, Uhlenbeck OC (2001) Evaluation of methylphosphonates as analogs for detecting phosphate contacts in RNA-protein complexes. *RNA* 7(4):622–631.
34. Noeske J, et al. (2015) High-resolution structure of the *Escherichia coli* ribosome. *Nat Struct Mol Biol* 22(4):336–341.
35. Erlacher MD, et al. (2005) Chemical engineering of the peptidyl transferase center reveals an important role of the 2'-hydroxyl group of A2451. *Nucleic Acids Res* 33(5): 1618–1627.
36. Labotka RJ, Omachi A (1988) The pH dependence of red cell membrane transport of titratable anions studied by NMR spectroscopy. *J Biol Chem* 263(3):1166–1173.
37. Rösch P, Kalbitzer HR, Goody RS (1980) 31P NMR-spectra of thiophosphate analogues of guanosine nucleotides: pH-dependence of chemical-shifts and coupling-constants. *FEBS Lett* 121(2):211–214.
38. Adamczyk AJ, Warshel A (2011) Converting structural information into an allosteric-energy-based picture for elongation factor Tu activation by the ribosome. *Proc Natl Acad Sci USA* 108(24):9827–9832.
39. Hamilton MG, Petermann ML (1959) Ultracentrifugal studies on ribonucleoprotein from rat liver microsomes. *J Biol Chem* 234(6):1441–1446.
40. Nakamura S, et al. (1978) Studies on polypeptide-chain-elongation factors from an extreme thermophile, *Thermus thermophilus* HB8. 3. Molecular properties. *Eur J Biochem* 92(2):533–543.
41. Wallin G, Kamerlin SC, Aqvist J (2013) Energetics of activation of GTP hydrolysis on the ribosome. *Nat Commun* 4:1733.
42. Maracci C, Peske F, Dannies E, Pohl C, Rodnina MV (2014) Ribosome-induced tuning of GTP hydrolysis by a translational GTPase. *Proc Natl Acad Sci USA* 111(40):14418–14423.
43. Erlacher MD, et al. (2006) Efficient ribosomal peptidyl transfer critically relies on the presence of the ribose 2'-OH at A2451 of 23S rRNA. *J Am Chem Soc* 128(13): 4453–4459.
44. Lang K, Erlacher M, Wilson DN, Micura R, Polacek N (2008) The role of 23S ribosomal RNA residue A2451 in peptide bond synthesis revealed by atomic mutagenesis. *Chem Biol* 15(5):485–492.
45. Polikanov YS, Steitz TA, Innis CA (2014) A proton wire to couple aminoacyl-tRNA accommodation and peptide-bond formation on the ribosome. *Nat Struct Mol Biol* 21(9):787–793.
46. Micura R (2002) Small interfering RNAs and their chemical synthesis. *Angew Chem Int Ed Engl* 41(13):2265–2269.
47. Ravikumar VT, Andrade M, Carty RL, Dan A, Barone S (2006) Development of siRNA for therapeutics: Efficient synthesis of phosphorothioate RNA utilizing phenylacetyl disulfide (PADS). *Bioorg Med Chem Lett* 16(9):2513–2517.
48. Kosutić M, et al. (2014) Surprising base pairing and structural properties of 2'-trifluoromethylthio-modified ribonucleic acids. *J Am Chem Soc* 136(18):6656–6663.
49. Frederiksen JK, Piccirilli JA (2009) Separation of RNA phosphorothioate oligonucleotides by HPLC. *Methods Enzymol* 468:289–309.
50. Lang K, Micura R (2008) The preparation of site-specifically modified riboswitch domains as an example for enzymatic ligation of chemically synthesized RNA fragments. *Nat Protoc* 3(9):1457–1466.
51. Mueller M, Wang M, Schulze-Briese C (2012) Optimal fine φ-slicing for single-photon-counting pixel detectors. *Acta Crystallogr D Biol Crystallogr* 68(Pt 1):42–56.
52. Kabsch W (2010) Integration, scaling, space-group assignment and post-refinement. *Acta Crystallogr D Biol Crystallogr* 66(Pt 2):133–144.
53. Olieric V, et al. (2009) A fast selenium derivatization strategy for crystallization and phasing of RNA structures. *RNA* 15(4):707–715.
54. Vagin A, Teplyakov A (2010) Molecular replacement with MOLREP. *Acta Crystallogr D Biol Crystallogr* 66(Pt 1):22–25.
55. Adams PD, et al. (2010) PHENIX: A comprehensive Python-based system for macromolecular structure solution. *Acta Crystallogr D Biol Crystallogr* 66(Pt 2):213–221.
56. Emsley P, Cowtan K (2004) Coot: Model-building tools for molecular graphics. *Acta Crystallogr D Biol Crystallogr* 60(Pt 12 Pt 1):2126–2132.

Supporting Information

Koch et al. 10.1073/pnas.1505231112

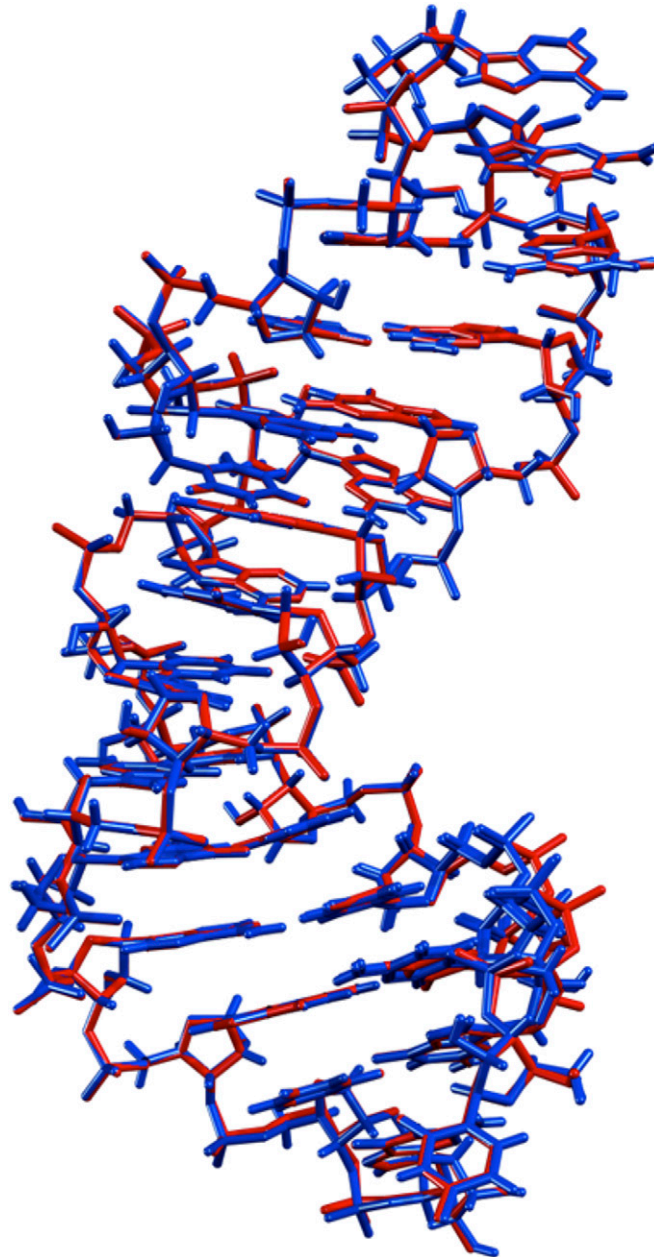


Fig. S1. Superposition of the unmodified SRL RNA (PDB ID code 3DVZ; red) and the 2'-OCH₃-G2661-mP-A2662 R_P methylphosphonate SRL RNA (PDB ID code 4Y27; blue); RMSD of 0.08 Å.

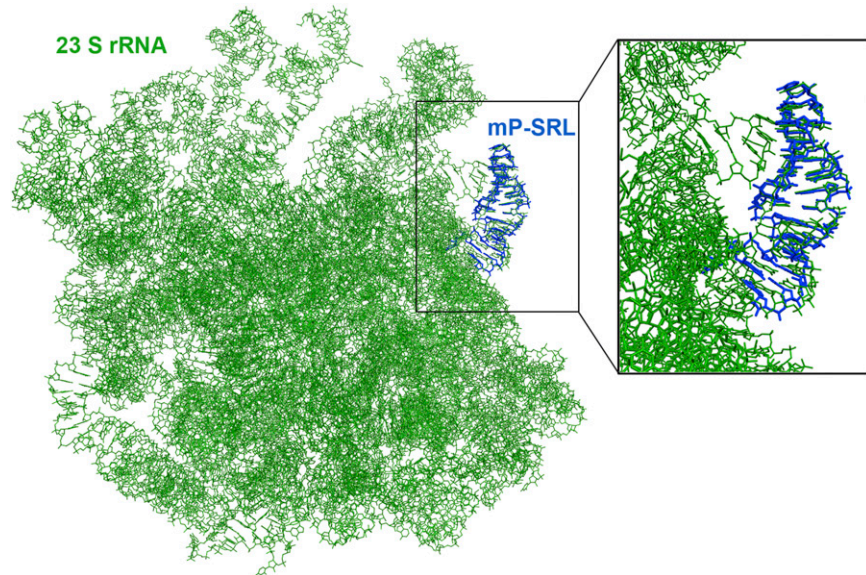


Fig. S2. Superposition of the 23S rRNA (within the context of the 70S ribosome; PDB ID code 4YBB; green) and the 2'-OCH₃-G2661-mP-A2662 R_P methylphosphonate SRL RNA (PDB ID code 4Y27; blue); RMSD of 0.84 Å.

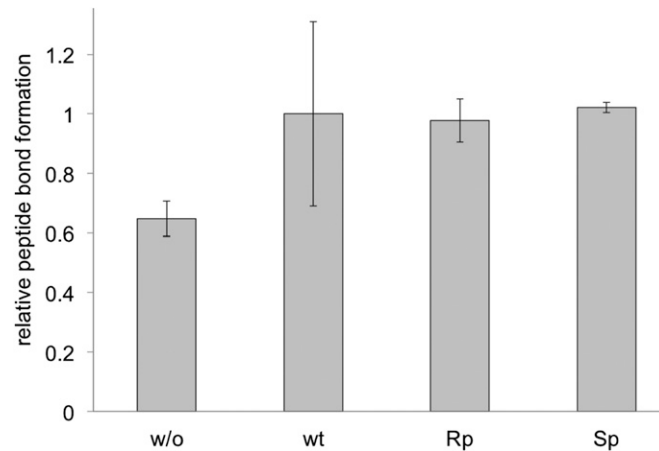


Fig. S3. Puromycin assay using SRL reconstituted ribosomes. Puromycin reaction to test for peptide bond formation activity and therefore correct assembly of reconstituted ribosomes was performed as described previously in ref. 1. Peptide bond formation of WT ribosomes was set to 1, and activities of modified SRL ribosomes are represented relative to WT. R_P and S_P refer to the two diastereomers of dG2661-mP-A2662-modified SRL oligonucleotides used for reconstitution. All SRL oligonucleotides (WT, R_P, and S_P) contained the U2466 mutation; w/o refers to reconstituted ribosomes that lack the SRL oligonucleotide and therefore provide a gap instead.

1. Erlacher MD, et al. (2005) Chemical engineering of the peptidyl transferase center reveals an important role of the 2'-hydroxyl group of A2451. *Nucleic Acids Res* 33(5):1618–1627.

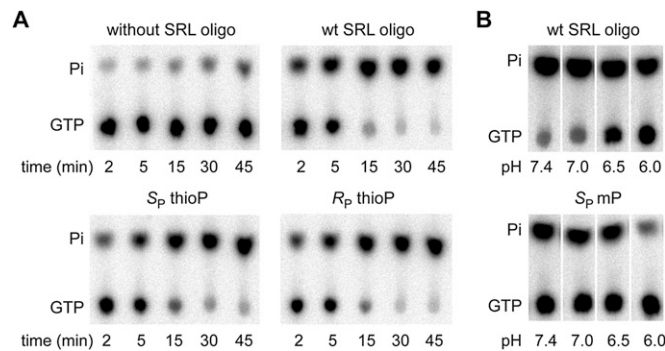


Fig. S4. Original TLC data referring to the graphs shown in Fig. 6: impact of A2662 *S_p* methylphosphonate SRL (A) and pH dependence of A2662 *S_p* methylphosphonate SRL (B) on EF-G GTP hydrolysis. (A) Uncoupled EF-G GTPase activity. TLC traces of a representative time course experiment using reconstituted ribosomes with the thiophosphate SRL modification. Three independent time course experiments have been performed and quantified to obtain means and SD shown in Fig. 6A. For uncoupled ribosome-stimulated EF-G GTP hydrolysis, 2 pmol reconstituted ribosomes (without SRL oligo, WT oligo, and both *S_p* and *R_p* thiophosphate diasteromers, respectively) were incubated with 15 pmol EF-G and 670 pmol GTP. Products were separated via TLC and visualized by phosphor imaging. Signals of radioactive GTP and Pi are indicated. (B) TLC traces for EF-G-stimulated GTP hydrolysis performed at different pH (7.4, 7.0, 6.5, and 6.0) after 30 min of incubation; 2 pmol of reconstituted ribosomes (WT and *S_p* methylphosphonate) were incubated with 15 pmol EF-G and 670 pmol GTP at different pH (as indicated). Products were separated via TLC and visualized by phosphor imaging. Three independent experiments have been performed and used for determination of means and SD shown in Fig. 6B.

Table S1. X-ray data collection and crystallographic refinement statistics

Data set	2'-OCH ₃ -G2661-mP-A2662
PDB ID code	4Y27
Space group	P4 ₃
<i>A</i> = <i>b</i> (Å)	29.50
<i>C</i> (Å)	77.15
Beamline	PX III - X06DA
Resolution range (Å)	30.00–1.00
Number of frames	5400
Oscillation angle	0.2°
Wavelength	0.77491
Average redundancy	39.1
Completeness*	99.8% (98.0%)
CC1/2*	100 (30.0)
Average I/σ*	35.15 (1.01)
Isa	32.5
<i>R/R</i> _{free}	13.5/14.9
Coordinate error (Å)	0.11

*Values for last resolution shell are shown in parentheses.